DOI: 10.7795/810.20260916
Recent developments in traceable dimensional measurements

Interferometric Methods for Groove Depth Calibration

L. Álvarez*, P. Etchepareborda, J. Campbell, N. Pérez and K. Bastida

Instituto Nacional de Tecnología Industrial, INTI, Av. Gral. Paz 5445, San Martín, Buenos Aires, Argentina

* *Corresponding author: ldalvarez@inti.gob.ar*

Abstract

Accurate characterization of shape, waviness, and roughness relies on traceable groove depth standards. A custom dual-wavelength Fizeau interferometer was developed to calibrate ISO 5436-1 type A1 groove material measures. Two interferometric methods were implemented: the fractional fringe method and a two-dimensional Fast Fourier Transform (FFT) phase retrieval method. A 5.75 µm nominal depth standard was measured and results were compared with stylus profilometry and a PTB reference value. Agreement within measurement uncertainties was achieved, demonstrating traceability to the SI metre and supporting the establishment of an interferometric primary standard for groove depth calibration.

1 Introduction

Surface metrology encompasses the characterization of shape, waviness, and roughness, covering dimensional scales from micrometres to nanometres. A wide range of measurement techniques is available, each based on different physical principles and suited to specific surface parameters. Among these, tactile stylus instruments remain the most widely used technique for two-dimensional (2D) profile roughness measurements [1]. In calibration laboratories, ensuring traceability of surface texture measurements requires periodic controls of key instrumental parameters such as vertical amplification, linearity and tip geometry. These characteristics are typically evaluated using step height material measures with standardized groove geometries spanning the instrument working range, allowing the response function to be assessed through interpolation of calibrated depths [2, 3]. However, the use of interferometric method for the calibration of groove material measures is still not widely implemented in regular calibration services.

At INTI, calibration services are provided in both dimensional metrology, such as flatness and gauge block calibration by interferometry, and surface texture metrology, including roughness and step height calibration. Ensuring traceability of groove depth material measures used for stylus instrument calibration is therefore essential to maintain a consistent measurement chain linked to the national length standard. In this context, a custom-designed Fizeau interferometer was adapted for multispectral (dual-wavelength) operation, enabling the calibration of the groove depth parameter, d, of ISO 5436-1 type A1 groove material measures [2], also referred to as Profile Groove Rectangular (PGR) material measures in ISO 25178-70 [3].

This work presents the implementation of two interferometric approaches for groove depth calibration: the fractional fringe method, consistent with interferometric length realization principles and gauge block calibration [4], and a method based on a two-dimensional Fast Fourier Transform (FFT) for full-field phase retrieval [5]. Both techniques were applied using two wavelengths traceable to the national length standard, ensuring traceability to the SI metre.

The proposed methodology was applied to the calibration of a type A1 groove depth standard with a nominal depth D of 5.75 µm. Results obtained using the interferometric methods are compared with those provided by stylus profilometry and a reference value from PTB (Physikalisch-Technische Bundesanstalt) to assess consistency between optical and contact techniques. This approach supports the extension of interferometric methods to the calibration of surface texture standards through a consistent traceability chain [6].

2 Experimental Setup

Figure 1(a) shows a schematic of the horizontally configured Fizeau interferometer used in this work. The sample is mounted vertically, with its working surface facing the object beam. The original setup, based on a 633 nm He-Ne laser and originally designed for routine flatness calibration, was modified by adding a second He-Ne laser source operating at 543 nm, enabling dual-wavelength (multispectral) measurements. Both interferometric techniques were applied using these two laser wavelengths, which are traceable to the national length standard through stabilized frequency references. The field of view can be adjusted by means of a zoom lens, allowing increased spatial resolution and the acquisition of interferograms such as the example shown in Figure 1(b). The groove depth standard GDS is calibrated against a λ/20 reference optical flat, ROF. This reference surface was previously characterized, and its residual flatness was considered in the uncertainty budget. No phase-shifting techniques were applied, and measurements were performed under static interferometric conditions.

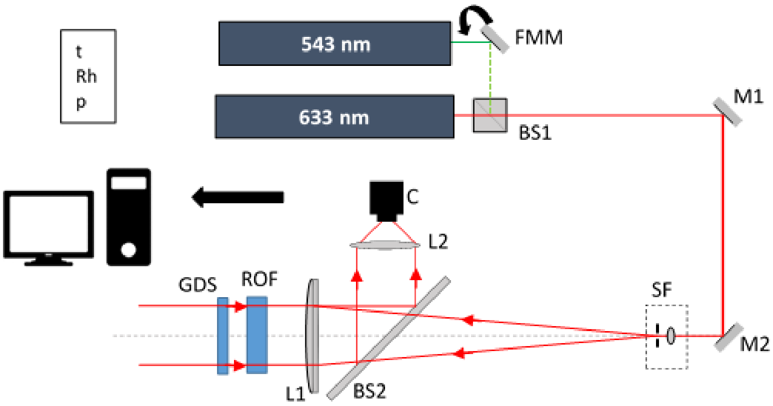

(a)

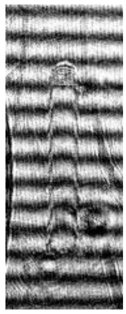

(b)

Figure 1. (a) Schematic of the adapted Fizeau interferometer used for multispectral measurements. FMM: flip mount mirror; BS1 and BS2: beam splitters; M1 and M2: mirrors; SF: spatial filter; L1: collimator; L2: zoom lens; C: camera; ROF: reference optical flat; GDS: groove depth standard. (b) Interferogram for λ =633 nm.

The artefact under study is a type A1 groove depth material measure (Federal Product Corp.) with a nominal depth *D* of 5.75 µm. The groove depth parameter *d*, corresponding to the calibrated value of the groove depth, was also measured using a stylus profilometer. At INTI, a Taylor Hobson TSI 120 instrument, equipped with Ultra software (version 6.1.12.1), is used for roughness calibration services. The instrument was calibrated for slope using angular gauge blocks. Groove depth measurements were performed at five positions along the standard, in accordance with the established calibration procedure, as shown in Figure 2.

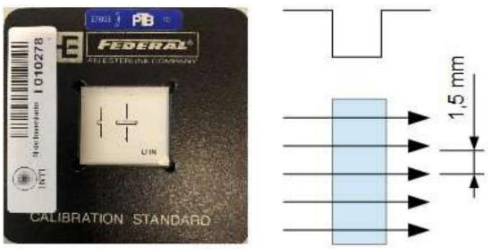

Figure 2. Groove depth standard, (nominal depth D 5.75 µm*) and measurement configuration using a stylus profilometer, indicating the evaluated positions.*

3 Interferometric Methods

3.1 Fringe Fraction Method

The groove depth parameter d is determined by applying the fractional fringe method to the interferograms, following procedures analogous to those used in gauge block interferometric calibration of [4]. This approach is consistent with interferometric length realization principles. Thus, the groove depth d, based on dual-wavelength approach, can be expressed as the average of the values obtained for each wavelength:

$$d = \frac{1}{2}\sum_{i=1}^{2}\frac{\lambda_i}{2}\left(K_i + f_i\right), \tag{1}$$

where λ_i is the wavelength in air, corrected for the refractive index, f_i is the average fractional fringe, and K_i is the integer fringe order associated with the nominal depth. The value of f_i is estimated from the average relative displacement of the interference fringes in the analysis regions. This displacement is obtained from the average intensity profiles extracted from three selected regions across the groove and featureless areas of the image processed interferogram for both wavelengths, as shown in Figure 3(a). The relative fringe displacement is determined by locating the minima of the averaged intensity profiles, which correspond to the fringe centres, Figure 3(b). The estimation considers all measurable fringe displacements within the groove, reducing the influence of noise and local surface irregularities.

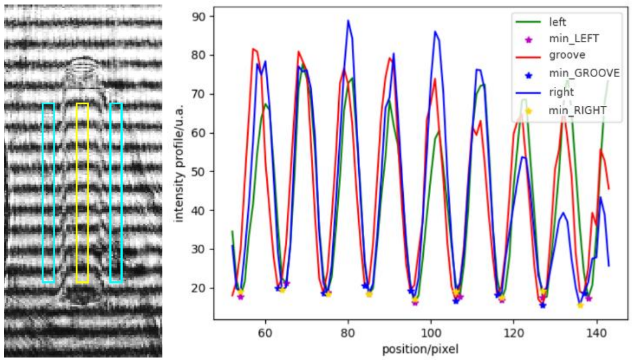

(a) *(b)*

Figure 3. (a) Interferogram for λ = 543 nm *with selected analysis regions and (b) corresponding intensity profiles extracted across the groove and adjacent flat regions.*

3.2 2D-FFT-Based Method

A second approach for d parameter measurement is based on the two-dimensional Fast Fourier Transform (FFT) of dual-wavelength interferograms [5]. Unlike the fringe fraction method, which employs images with low spatial fringe density, the FFT method requires a significant tilt between the object and reference beams. This induces a high-density fringe pattern that acts as a modulated spatial carrier. The technique leverages high-frequency components to demodulate full-field phase information across the entire image. Specifically, the phase is retrieved from the complex Fourier spectrum by isolating a first-order diffraction component, shifting it to the origin of the Fourier domain through numerical multiplication with the conjugated spatial carrier, and applying an inverse FFT. The resulting phase map, typically wrapped phase within the range [-π, π) rad, undergoes an unwrapping process to reconstruct a continuous phase distribution representing the surface topography. Assuming an ideal planar reference wavefront, the retrieved phase is proportional to the topography by a factor of λ/4π. The corresponding measurement model is analogous to Eq. (1),

$$d = \frac{1}{2}\sum_{i=1}^{2}\frac{\lambda_i}{2}\left(K_i + \frac{\Delta\varphi_i}{2\pi}\right), \tag{2}$$

where $\Delta\varphi_i$ is the phase difference between the groove region and the average phase of the adjacent zones. In this work, it is defined as:

$$\Delta\varphi_i = \varphi_{ig} - \frac{1}{2}\left(\varphi_{il} + \varphi_{ir}\right), \tag{3}$$

where φ_{ig} is the mean phase in the groove region, and φ_{il} and φ_{ir} are the mean phase values in the left and right adjacent regions respectively, for each wavelength λ_i.

Figure 4(a) to (c) displays the interferogram, the reconstructed phase map, and the mean profile extracted along the groove, respectively. From this profile, the groove depth parameter d is determined by evaluating the height difference between the groove region and the adjacent reference regions, following the guidelines of ISO 25178-70 [3] and [7]. The increased data density provided by this approach facilitates a detailed visual interpretation of the topography, thereby reducing the likelihood of biased measurements. Consequently, the measurements are less sensitive to local anomalies or sample orientation, offering a more robust and stable representation of the actual surface state.

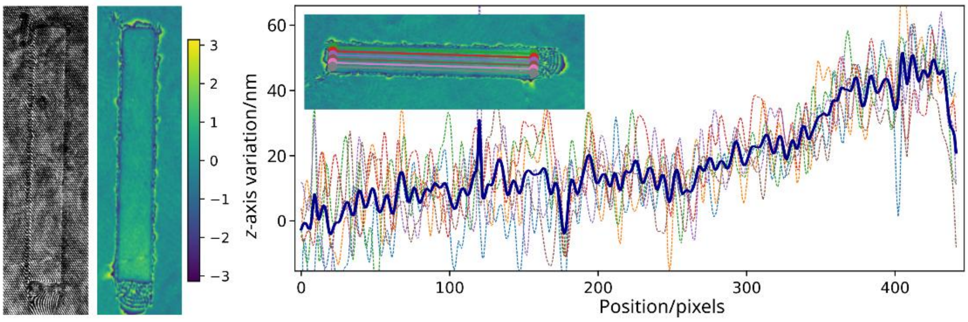

(a) *(b)* *(c)*

Figure 4. (a) Interferogram for λ = 543 nm, *(b) reconstructed whole-field phase map using FFT-based method, and (c) mean profile extracted along the groove.*

4 Uncertainty Budgets

4.1 Fringe Faction Method

The combined standard uncertainty was evaluated in accordance with the Guide to the Expression of Uncertainty in Measurement, GUM [8]. From the uncertainty evaluation perspective, several contributions associated with the measurement model, given by Eq. (1), must be considered. These include effects related to beam obliquity, wavefront deviations of the reference optical flat ROF, and corrections due to the refractive index of air, evaluated using the Edlén equation [9]. The expected values of these influence quantities are assumed to be zero; however, their associated standard uncertainties are non-zero and contribute to the combined standard uncertainty $u(d)$. The ROF contribution was conservatively modelled as an additive influence quantity with unit sensitivity coefficient, assuming no spatial correlation between measurement regions and a rectangular distribution derived from the calibrated peak-to-valley flatness (9 nm), obtained in the same laboratory using the three-flat test. Table 1 summarizes the individual uncertainty components considered in the groove depth measurement, including the corresponding sensitivity coefficients. The combined standard uncertainty is expressed using the $Q[a, b]$ notation [4, 10], where a represents depth-independent (end effects) contributions arising from the local surface characteristic of the GDS and its interactions with the measurement system, and b represents depth-dependent contributions associated with the bulk properties of the GDS and the environmental conditions affecting the measurement. Thermal contributions were found to be negligible compared with the contributions associated with fringe localization and optical effects.

Table 1: Standard uncertainty components for depth groove measurement by fringe fractional method.

Component	Source	Standard uncertainty $u(x_j)$	$\lvert c_{x_j} \rvert$	u_{x_j}/nm
Fringe fractional method	Wavelength, λ_1	1.50 x 10^{-4} nm	7.9 x 10^{-4} D/nm	1.18 x 10^{-7} D
	Wavelength, λ_2	8.00 x 10^{-5} nm	9.2 x 10^{-4} D/nm	7.35 x 10^{-8} D
	Fringe fraction, f_1	0.0173 fringe	158.25 nm	2.74 nm
	Fringe fraction, f_2	0.0173 fringe	135.88 nm	2.35 nm
Thermal effects	GDS temperature, t_{GDS}	0.252 °C	3.3 x 10^{-6} D/°C^{-1}	8.31 x 10^{-7} D
	Thermal expansion, α	1.91 x 10^{-7} °C^{-1}	0.5 D °C	9.53 x 10^{-8} D
Interferometric optics	Wavefront, δ_{ROF}	5.2 nm	1	5.2 nm
	Source size, $\delta_{\Omega 1}$	1.15 µm	2.22 x 10^{-4} D/m	2.57 x 10^{-10} D
	Alignment, $\delta_{\Omega 2}$	0.5 mm	1.26 x 10^{-4} D mm^2	3.14 x 10^{-5} D
Air refractive index	Air temperature, n_t	0.25 °C	9.12 x 10^{-7} D/°C	2.29 x 10^{-7} D
	Air pressure, n_p	7.57 Pa	2.66 x 10^{-9} D/Pa	2.02 x 10^{-8} D
	Humidity, R	2.5 %	9.8 x 10^{-9} D	2.46 x 10^{-8} D
	Edlén equation, E	1.00 x 10^{-8}	D	1.00 x 10^{-8} D
		Combined standard uncertainty		$u(d) = Q[6.3 \text{ nm}, 3.14 \text{ x } 10^{-5}\, D]$

It can be observed that the dominant contributions arise from the wavefront deviation of the ROF and from the estimation of the fractional fringe values. This includes contributions from digital image processing and fringe localization, as discussed in [11]. The standard uncertainties associated with the factional fringe values f_i were estimated from the statistical dispersion of repeated evaluations, expressed as typical standard deviation (Type A contribution, [8]). Although, in principle, different uncertainty values could be expected for each wavelength due to variations in interferogram contrast and intensity distribution, in this work both contributions were assumed to be equal as an approximation, since no significant differences were observed within the experimental conditions.

On the other hand, among the D-dependent contributions, the alignment term shows a significant contribution. This can be attributed to the need to adjust the pinhole position when switching between wavelength, as the alignment procedure. Possible correlations between quantities derived from the same interferogram were considered negligible.

4.2 2D-FFT-Based Method

An estimation of the uncertainty was also conducted following the GUM framework [8], using an uncertainty budget consistent with that applied to the fringe fraction method. The main difference was that the contributions from the FFT-based method correspond to phase difference estimates according to Eq. (2). Furthermore, the alignment uncertainty is higher due to the intentional misalignment required to generate the spatial carrier. For a tilt angle of 0.5°, estimated from the spatial frequency of the fringe pattern, the resulting alignment uncertainty contribution is $1.1 \times 10^{-4} D$.

The experimental standard deviation of the phase, $s_{\varphi(l,g,r)i}$, accounts for spatial phase variability within each region, with contributions from both measurement noise and local surface topography. Therefore, the spatial phase variability contribution of the method, $u_{\text{spatial},\Delta\varphi_i}$, to the uncertainty $u(d)$ was calculated from the estimated experimental standard deviation of the average phase value within each analysed region

$$u_{\text{spatial},\Delta\varphi_i} = \frac{\lambda_i}{8\pi}\sqrt{\frac{s^2_{\varphi_{li}}}{4n_{\text{eff},l}} + \frac{s^2_{\varphi_{gi}}}{n_{\text{eff},g}} + \frac{s^2_{\varphi_{ri}}}{4n_{\text{eff},r}}}, \quad (5)$$

where $n_{\text{eff},l}$, $n_{\text{eff}.g}$ and $n_{\text{eff},r}$ are the effective numbers of independent pixels in each region. A conservative reduction factor of 5 was applied to account for residual spatial correlation arising from FFT phase reconstruction and local topography, resulting in $n_{\text{eff},(l,g,r)} = n_{(l,g,r)}/5$.

A set of 20 images corresponding to the same field of view with the groove was processed to estimate the average phase difference $\overline{\Delta\varphi_i}$, the root mean square (RMS) spatial uncertainty contribution $u^{RMS}_{\text{sp},\Delta\varphi_i}$, and a repeatability contribution associated with the estimation of $\overline{\Delta\varphi_i}$. The repeatability contribution was evaluated as $u_{rep_i} = \frac{s_{\Delta\varphi_i}}{\sqrt{20}}$, where $s_{\Delta\varphi_i}$ is the experimental standard deviation of $\Delta\varphi_i$ across the 20 analysed frames. The obtained uncertainty contributions for each wavelength were: $u^{RMS}_{\text{sp},\Delta\varphi_1} = 0.33$ nm, $u^{RMS}_{\text{sp},\Delta\varphi_2} = 0.39$ nm , $u_{rep_1} = 0.03$ nm and $u_{rep_2} = 0.05$ nm . Finally, the combined standard uncertainty was $u(d) = Q[5.6 \text{ nm}, 1.4 \text{ x } 10^{-4}\, D]$ which, for the measured groove depth $D = 5.75$ µm results in $u(d) = 5.7$ nm.

4.2.1 Sensitivity Coefficients for the Optical System Contribution

A complementary uncertainty analysis was conducted to evaluate the validity of assuming a unit sensitivity coefficient for the optical system contribution, primarily associated with the flatness calibration of the reference optical flat. This analysis was performed using a Monte Carlo framework based on synthetic interferograms. The simulated interferograms incorporated various stochastic and deterministic effects, including:

- **Image acquisition parameters:** Poisson-distributed intensity noise and camera quantization effects.
- **Sample characteristics:** Number of grooves, aspect ratio, and angular orientation.
- **Optical system imperfections:** Aberrations arising from misalignments, non-ideal components (including reference flat topography and transmission distortions), and localized defects such as scratches.

Thermal effects, specifically GDS temperature variations and material linear thermal expansion, were excluded from this specific analysis.

A total of 1000 samples were simulated with the same aspect ratio and nominal depth as our GDS, assuming a groove depth tolerance of 100 nm with a uniform distribution. Two images per sample were synthetized following the proposed dual wavelength scheme. A synthetic interferogram is shown for illustrative purposes in Figure 5. Each pair of images was automatically processed to estimate the groove depth parameter d for each sample. Optical aberrations arising from non-ideal components were simulated by introducing non-planar input wavefronts at the image plane for both object and reference beams. These wavefronts were constructed using random Zernike polynomials up to 5$^{\text{th}}$ order, with coefficients progressively reduced by a factor of two for each increasing order. This approach produced aberrated wavefronts associated with low-pass filtered surfaces exhibiting flatness deviation consistent with ISO 12781-1 [12]. The overall amplitudes of the wavefronts were scaled such that the resulting maximum optical path difference was consistent with the calibrated flatness deviation of the reference optical flat (9 ± 23) nm. A few examples of the resulting aberration phase maps are shown for illustrative purposes in Figure 6. The simulated images were contaminated with different noise sources to avoid underestimating their effects in the performance assessment. The simulated environmental conditions were T = (20 ± 1) °C, RH = (50 ± 5) %, P = (1015.9 ± 15) hPa, assuming normal distributions for temperature, relative humidity and air pressure, respectively.

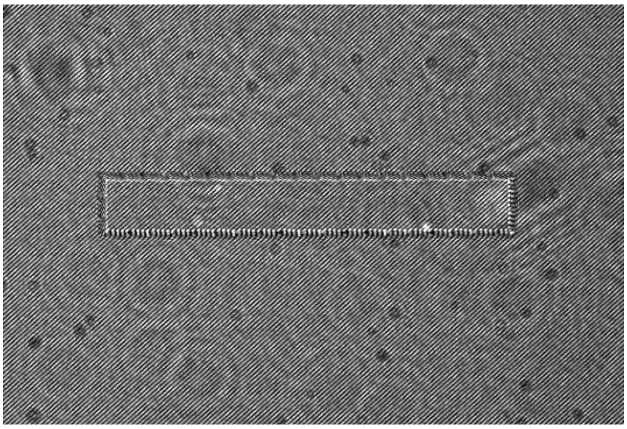

Figure 5. Example of a synthetic interferogram for $\lambda = 543$ nm.

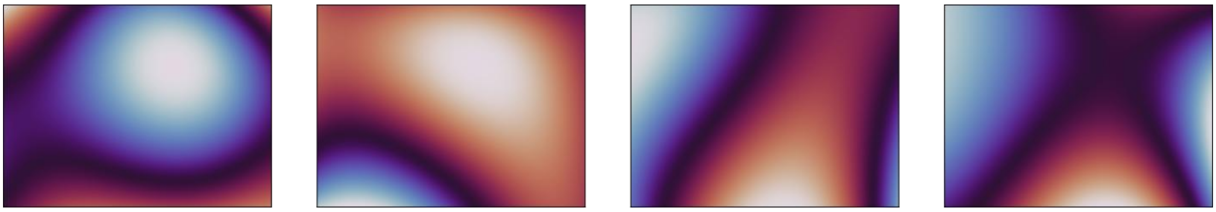

Figure 6. Examples of phase maps corresponding to synthetic wavefront aberrations generated from the simulated optical system (using random Zernike coefficients up to 5th order). The colormap scales were intentionally omitted, but they are roughly equivalent and span a range of ± 0.2 rad.

The root mean square error (RMSE) in the estimation of d was considered as the combined standard uncertainty contribution associated with all simulated effects, yielding u_{MC} = 0.45 nm, with a 95th percentile of the simulated error distribution was 0.85 nm. These values are significantly smaller than the simulated wavefront distortions. Therefore, assuming a unit sensitivity coefficient is not appropriate for estimating the corresponding uncertainty contribution.

Four additional simulations were conducted to estimate the sensitivity coefficient associated with aberrations introduced by the optical components. The amplitudes of the aberrations were varied to values, v_{ROF}, corresponding to optical flats with flatness deviation of $[0.5, 0.75, 1, 1.5, 2]$ x 9 nm, with a constant uncertainty of flatness deviation u_{ROF} = 23 nm, k = 1. A linear regression model, $u_{MC}^2 = c_{ROF}^2\, v_{ROF}^2 + A$ was used to estimate the sensitivity coefficient c_{ROF}, where the actual calibrated flatness deviation of the ROF was treated as an uncertainty contribution. The estimated sensitivity coefficient was $c_{RP} = 6.5 \times 10^{-3}$, resulting in a combined standard uncertainty $u(d) = Q[0.43 \text{ nm}, 1.4 \text{ x } 10^{-4}\, D]$, which yields $u(d) = 0.9$ nm.

5 Results and Analysis

The average groove depths obtained using the two interferometric methods and stylus instrument were compared with the value reported in the PTB calibration certificate which was adopted as the reference value (RV_{PTB}). Table 2 summarizes the results obtained with each method together with the associated expanded uncertainties and reference value.

Table 2: Results obtained for each method and reference value.

Item	Nominal groove depth $D/\mu m$	Method	Measured groove depth $d/\mu m$	Expanded uncertainty $U/\mu m$ $(k = 2)$
Federal Product Corp.	5.75	Fringe fraction	5.724	0.013
		FFT-based	5.721	0.002
		Stylus profilometry	5.71	0.04
		PTB (RV_{PTB})	5.73	0.02

The comparison was performed following the general guidelines established by the CIPM-CCL for key comparisons [13, 14]. For each method, the degree of equivalence with respect to RV_{PTB} was evaluated. The associated uncertainty budgets included a contribution accounting for the correlation arising from measurements performed on the same groove depth standard. In the case of stylus profilometry, a larger correlation contribution was assumed, since the reference value and the measurement result rely on the same measurement principle. The interferometric results show good agreement with the reference value within the stated uncertainties. Among the evaluated approaches, the FFT-based method provides the lowest estimated uncertainty.

Figure 7 shows the comparison results with respect to RV_{PTB}, together with the corresponding normalized errors, E_n. All evaluated E_n values are below unity, indicating agreement between the measurement results and the reference value within the stated uncertainties. Overall, a good consistency is observed among the different measurement approaches.

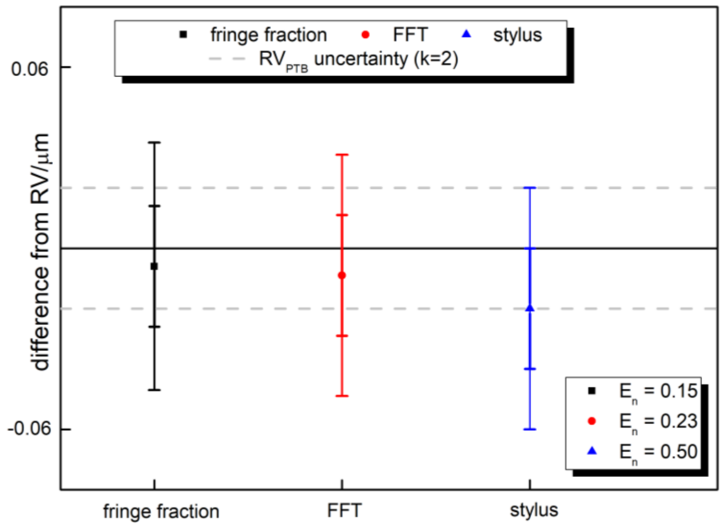

Figure 7. Comparison results for the fringe fraction method, FFT-based method, and stylus profilometry with respect to RV_{PTB}. The normalized errors, E_n, are indicated for each method. Thick error bars represent the combined standard uncertainty (k=1), while thin error bars correspond to the expanded uncertainty for k = 2. Dashed horizontal lines indicate the expected uncertainty internal associated with RV_{PTB}.

These results indicate that the adapted Fizeau interferometer is suitable for use as a primary optical method for groove depth calibration. The obtained agreement with the reference value supports its application for establishing the metrological traceability of stylus profilometry to the national length standard, thereby contributing to the closure of INTI's roughness traceability chain.

5.1 Limitations and Traceability Considerations

Both the FFT-based method and the fractional fringe method reveal measurable variations of the groove depth along the longitudinal direction of the artifact, even though the former provides a more localized evaluation. This indicates that the definition of the measurand, the groove depth parameter d, depends on the evaluation strategy, which may lead to systematic differences between methods. Additionally, edge effects at the groove boundaries may influence both fringe-based and stylus measurements, particularly in regions where the groove boundaries deviate from an ideal step profile and exhibit gradual transitions. Thus, differences between optical and stylus-based measurements can be attributed to the distinct interaction mechanisms with the surface, particularly in the presence of local defects or boundary effects.

From the traceability perspective, the optical measurements are primarily linked to the wavelengths of the laser sources, which are traceable to the national length standard through stabilized frequency references. However, the realized groove depth obtained by interferometric methods also depends on the reference optical flat (ROF), whose residual wavefront deviations contribute to both the measurement result and its uncertainty. Therefore, traceability is established not only through the laser wavelengths, but also through the characterization and stability of the reference surface. This characterization is performed using the three-flat method, based on interferometric measurements traceable to stabilized frequency references. Since both the reference surface characterization and the groove depth measurements are performed using the same interferometric system, a certain degree of correlation is expected. However, its contribution to the combined uncertainty is assumed to be negligible due to different processing procedures and measurement configurations involved.

Additional limitations arise from the image processing stage, including fringe detection and phase retrieval algorithms, which may introduce method-dependent biases. These effects are partially mitigated by averaging over multiple regions and by using of dual-wavelength techniques to resolve fringe-order ambiguity.

6 Conclusion

This work contributes to strengthening the link between dimensional and surface texture metrology through two traceable interferometric methods. It presents the adaptation of a custom-designed Fizeau interferometer for dual-wavelength operation. This system enabled the implementation of two measurement techniques, the fractional fringe method and the FFT-based method, for the calibration of type A1 groove depth standards. The results show good agreement with stylus profilometry and with the reference value provided in the PTB calibration certificate. All evaluated normalized errors E_n were below unity, confirming agreement among the different measurement approaches within the stated uncertainties.

The analysis also highlights that groove depth should be interpreted as an operationally defined measurand, whose depth parameter d depends on the evaluation strategy and the interaction between the measurement system and the surface. In particular, deviations from ideal step geometry, such as gradual transitions at the groove boundaries, can introduce systematic differences between optical and stylus-based methods.

From a traceability perspective, the optical measurements rely not only on the wavelength of the laser sources but also to the characterization and stability of the reference optical flat, which may represent the dominant contribution to the combined standard uncertainty of the groove depth.

The results support the suitability of the adapted Fizeau interferometer as a traceable optical method for groove depth calibration, providing a reliable route for establishing traceability to the SI metre through wavelength-based measurements. Consequently, this approach supports the establishment of metrological traceability of stylus profilometry to the national length standard, contributing to the closure of INTI´s roughness traceability chain at. Future work will focus on extending the methodology to additional surface texture standards and on further characterizing the uncertainty contributions associated with the optical arrangement, image processing, and reference surface characterization.

References

[1] Whitehouse D 2010 Handbook of Surface and Nanometrology *CRC Press*

[2] ISO 5436-1 2000 Geometrical product specifications (GPS) - Surface Texture: Profile method; Measurement Standards. Part 1: Material Measures *International Organization for Standardization*

[3] ISO 25178-70 part 70 2014 Geometrical product specifications (GPS) - Surface Texture: Areal - Part 70: Material Measures *International Organization for Standardization*

[4] Decker J et al. 1997 Uncertainty evaluation for the measurement of gauge blocks by optical interferometry *Metrologia* 34(6), 479-493

[5] Takeda, M et al. 1982 Fourier-transform method of fringe pattern analysis for computer-based topography and interferometry *J. Opt. Soc. Am.*, *72*(1), 156-160.

[6] Pappas A et al. 2023 Review of material measures for surface topography instrument calibration and performance verification *Meas. Sci. Tech*. 35 012001

[7] de Groot P 2015 Principles of interference microscopy for measurement of surface topography *Advances in Optics and Photonics* 7(1), 1-65

[8] JCGM 100:2008 Evaluation of Measurement Data – Guide to the Expression of Uncertainty in Measurement (GUM)

[9] Birch K et al. 1994 Correction to the updated Edlén equation for the refractive index of air *Metrologia* 31, 315-316

[10] BIPM KCDB Office 2020 Conversion of equations for KCDB *BIPM*

[11] Yapur F et al. 2013 Estimación de incertidumbres en el procesamiento digital de imágenes, asociada a la medición interferométrica de desvío de planitud *Anales AFA* 24(1), 47-50

[12] ISO12781-1:2011 Geometrical product specifications (GPS) - Flatness - Part 1: Vocabulary and parameters of flatness *International Organization for Standardization*

[13] CIPM 2019 CIPM MRA-G-11: Guidance on the implementation of key comparison linking BIPM

[14] Cox M 2002 The evaluation of key comparison data *Metrologia* 39(6),589-595